Asian Journal of Chemistry; Vol. 37, No. 10 (2025), 2449-2454
ASIAN JOURNAL OF CHEMISTRY
https://doi.org/10.14233/ajchem.2025.34344

Thioacetamide-Doped Zinc Nitrate Hexahydrate Nanostructures: Hydrothermal Synthesis and Characterization

ANAND GASPAR[1,2], M. PACKIYA RAJ[3], A. VENKATESAN[4], ANTONY LAWRENCE ANDREWS[5], SAVARIMUTHU DAVID AMALRAJ[2], C. PALANIVEL[1,*] and M. SATHISH[6,*]

[1]PG & Research Department of Chemistry, Government Arts College, C. Mutlur, Chidambaram-608102, India
[2]PG & Research Department of Chemistry, St Joseph's College of Arts & Science (Autonomous), Cuddalore-607001, India
[3]PG & Research Department of Physics, Loyola College, Chennai-600034, India
[4]PG & Research Department of Mathematics, St Joseph's College of Arts & Science (Autonomous) Cuddalore-607001, India
[5]Department of Physics, School of Natural and Physical Sciences, The University of Papua New Guinea, P.O. Box 320, Waigani Campus, Port Moresby, National Capital District 134, Papua New Guinea
[6]PG & Research Department of Physics, St Joseph's College of Arts & Science (Autonomous), Cuddalore-607001, India

*Corresponding authors: E-mail: palanivelchem@gmail.com; sathishmary2013@gmail.com

Received: 26 June 2025 *Accepted*: 10 September 2025 *Published online*: 30 September 2025 AJC-22128

In this study, we successfully synthesized thioacetamide-doped zinc nitrate hexahydrate nanostructures using a hydrothermal method. Thioacetamide was used as a dopant in order to improve the desirable structural, optical, morphological and electrochemical properties. The synthesized materials were characterized various analytical techniques. In particular, UV–visible spectroscopy was employed to investigate the optical absorption properties and the effects of thioacetamide doping, which revealed corresponding changes in the band gap. FTIR analysis confirmed the functional groups and chemical bonding within the material. X-ray diffraction (XRD) verified its crystalline structure and phase purity, while scanning electron microscopy (SEM) revealed surface morphology. X-ray photoelectron spectroscopy (XPS) provided insights into elemental composition and oxidation states, confirming the successful incorporation of thioacetamide as a dopant. Electrochemical characterization *via* cyclic voltammetry (CV) demonstrated enhanced redox activity resulting from thioacetamide doping. And its electrochemical performance is evaluated using galvanostatic charge-discharge (GCD) analysis. The results demonstrate that hydrothermal synthesis is an effective method for producing doped zinc-based nanostructures with enhanced or tunable properties. Importantly, understanding and predicting the tunable properties of the material can facilitate its use in a wide range of future optoelectronic and electrochemical applications

Keywords: Cyclic voltammetry, Thioacetamide, Hydrothermal, X-ray photoelectron spectroscopy, XRD.

INTRODUCTION

One factor that leads to the increased interest in zinc nitrate as a precursor to complex functional materials is its high solubility and reactivity, stability and manipulation [1]. The thermal decomposition of zinc nitrate showed that it is hydrothermally stable, has decent kinetics of decomposition and allows many different dopants to modify a variety of structural, optical and electrochemical properties [2,3]. When a sulfur precursor was added, such as thioacetamide, then zinc nitrate led to a new group of functional nanostructured materials that have interest in fields of biocatalysis, energy storage, sensor technologies and optoelectronics. As a versatile and highly soluble and reactive aqueous precursor zinc nitrate hexahydrate, could be incorporated into nanomaterials using methods of doping for modifications to achieve desired properties [4,5]. The incorporation of dopants into zinc precursor based systems is an established practice, done with a pronounced aim towards materials for targeted applications.

Thioacetamide (TAA) is a sulphur and organosulfur compound that we consider a well documented dopant and source of sulphur for changing the structural and electronic environment of zinc-based nanomaterials [6,7]. The hydrothermal doping of zinc nitrate with thioacetamide produced unique nanostructured examples produced usually with favourable optical absorption capacity or an interesting structure morphology as

well as reasonable variation in degradation after use in electrochemical experimentation [8,9]. Such materials hold significant promise for future applications across key scientific fields, including catalysis, sensing and energy storage particularly in systems involving zinc nitrate derived from oxidized biomasses [10,11]. The emergence of zinc-based compounds has gained interest and attention due to its unique physical and chemical features, cost efficiency, sustainable environmental attributes and a range of possible applications in electronics, catalysis, energy storage and environmental remediation vision.

Zinc nitrate hexahydrate is a widely used and attractive precursor for the synthesis of semiconductors such as ZnO and other zinc-based nanomaterials [12-14]. Zinc nitrate is soluble and reactive with aqueous samples and solutions of which many processes can be used to formulate controllable solubility (*e.g.* hydrothermal or solvothermal) and reactivity (*e.g.* heat up cycle, microwave with or without pressure or combination). Doping is considered a common and effective way to amend intrinsic fundamental properties of base materials, which generates the doped functionality of material [15-17]. This process involves other foreign atoms and/or molecules that are bouned to establish known structure and enhance configurational, aqueous and electronic surface. Thioacetamide, an organosulfur compound, has also been evaluated for use as a dopant and sulfur source in zinc nitrate [18-21]. Thioacetamide would decompose under hydrothermal conditions forming H_2S in the gaseous phases to help incorporation of sulfur or sulfur based moieties into the zinc nitrate matrix to maintained levels which would change the crystal structure, band gap energy and electronic states in bad ways that would negatively affect the functional performance of materials prepared [22].

Under high kinetic interaction between zinc nitrate and thioacetamide, nanostructured materials with enhanced electronic properties such as optical absorption, electrical conductivity and electrochemical activity were synthesized. These enhancements, attributed to the reaction kinetics, present significant advantages for emerging technologies, including gas sensing, photocatalysis, electrochemical energy storage, antimicrobial activity and optoelectronic applications.

EXPERIMENTAL

All reagents used for the synthesis were of analytical grade and used without further purification. In this work, zinc nitrate hexahydrate ($Zn(NO_3)_2{\cdot}6H_2O$) as zinc source, thioacetamide (CH_3CSNH_2) as sulfur dopant, deionized water as solvent and ammonia solution (NH_4OH) for pH adjustment.

Characterization: The FT-IR spectra was recorded using an IR-550 spectrometer with KBr pellets (Toronto Area, ON, Canada). X-ray diffraction (XRD) patterns were obtained using a Philips X'Pert Pro-MPD diffractometer (Eindhoven, Netherlands) equipped with Cu*K*α radiation (λ = 0.15406 nm) as the X-ray source. The optical characteristics were analyzed using a UVD-2950 double-beam UV-Vis spectrophotometer over the wavelength range of 200–800 nm. Surface morphology was investigated by scanning electron microscopy (SEM) using a Mira3 model instrument (TESCAN). The elemental composition analysis was conducted utilizing X-ray photoelectron spectroscopy (XPS) using a monochromatic Mg*K*α radiation (1253.6 eV) X-ray source for the analysis.

Hydrothermal synthesis of thioacetamide doped zinc nitrate: Thioacetamide-doped zinc nitrate hexahydrate nanostructures were synthesized *via* the hydrothermal method, which facilitates controlled nucleation and growth of doped nanomaterials under high pressure and elevated temperature. The synthesis process employed three molar ratios of thioacetamide to zinc nitrate: 0.0 (HZ0: undoped), 0.2 mol (HZ2) and 0.3 (HZ3).

Preparation of precursor solution: A 0.1 M solution of $Zn(NO_3)_2{\cdot}6H_2O$ was mixed with thioacetamide (TAA) at varying molar ratios (0.0, 0.2, and 0.3 relative to $Zn(NO_3)_2$) under constant magnetic stirring for 30-45 min. Due to the hydrolytic instability of thioacetamide, agitation promotes the release of H_2S, introducing sulfur into the system and altering the chemical environment around the zinc ions. Then, the homogenous mixture was transferred to a Teflon-lined stainless-steel autoclave and filled to 70-80% of total volume to maintain pressure throughout the reaction.

Hydrothermal treatment: The autoclave was then sealed and placed into a hot air oven set at 160 ºC for 6 h. The temperature and pressure conditions used during synthesis were suitable for controlling the size of the doped zinc nitrate based phases formed through nucleation and growth. The autoclave was then allowed to cool passively to room temperature, after the reaction was considered complete. The resulting precipitate was collected *via* centrifugation or through filtration. To remove any unreacted precursors and byproducts the precipitate was washed several times with deionized water and ethanol prior to drying in a hot air oven at 80 ºC for more than 6 h. Lastly, if necessary, the dried material was to be calcined at 200-300 ºC for 2 h, to try and improve the crystallinity and remove any remaining organic contaminants.

RESULTS AND DISCUSSION

XRD analysis: The X-ray diffraction (XRD) analysis was carried out to evaluate the crystal structure, phase composition and crystallite size of the synthesized thioacetamide-doped zinc nitrate hexahydrate nanomaterials ($Zn(NO_3){\cdot}6H_2O$-C_2H_5NS). The XRD patterns of the sample is presented in the Fig. 1, revealing sharp and well-defined peaks at 2θ values of 31.581º, 34.249º, 36.057º, 47.785º, 56.508º, 62.836º and 67.649º, which correspond to the (100), (002), (101), (102), (110), (103) and (112) crystallographic planes, respectively. Furthermore, the peaks observed at 28.1º, 44.2º, 47.1º and 56.1º in the HZ0 sample indicate the presence of undoped zinc within the material. The diffraction peak positions and their associated Miller indices closely match those in the standard JCPDS card No. 36-1451, confirming the formation of a hexagonal quartzite structure characteristic of ZnO. These results demonstrate that zinc nitrate undergoes thermal decomposition under hydrothermal conditions, with thioacetamide facilitating the *in situ* formation of ZnO nanocrystals.

The most prominent diffraction peak, located at 36.057º (101 plane), represented the expected orientation of the structured nanocrystals. Peak intensity and sharpness indicated a well-developed crystalline phase. The absence of additional

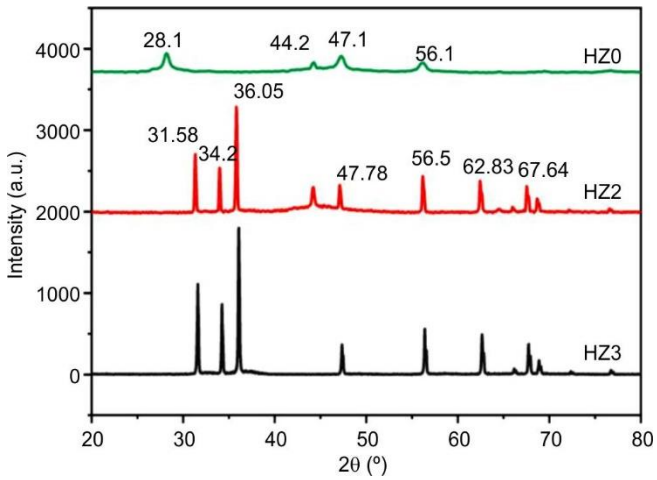

Fig. 1. XRD spectra of thioacetamide-doped zinc nitrate hexahydrate nanostructures

unidentified diffraction peaks in the pattern excludes the possibility of secondary phases (*e.g.* ZnS, $Zn(OH)_2$, unreacted thioacetamide) and verifies that doping of thioacetamide resulted in no contaminants or secondary phases, which indicated that thioacetamide incorporated into the ZnO lattice.

When added during hydrothermal synthesis, thioacetamide, a source of sulfur, can modify the ZnO crystal structure. The ionic radius of sulfur (S^{2-} = 1.84 Å) is slightly larger than that of oxygen (O^{2-} = 1.40 Å). The incorporation of sulfur by substitution for oxygen in the ZnO lattice or occupancy of interstitial sites can induce local lattice distortions, which would affect the diffraction pattern on an insignificant scale. This study revealed small shifts of peak position and peak intensity correspondingly when compared to pure ZnO, possibly as a result of slight lattice strain or distortion from sulfur inclusion. The crystallite size can be calculated by using the (101) peak at 36.057º revealing that crystallite size should be in the nanometer size range, which gives evidence of the formation of nanocrystalline material. The sharpness of the peaks substantiates the crystalline size and confirms the high crystallinity and homogeneity of the synthesized nanostructures.

The presence of thioacetamide might also incorporate intrinsic point defects such as zinc interstitials (Zn_i), oxygen vacancies (V_O), or sulfur-defect sites in ZnO. Defects have been shown to play an important role in altering and enhancing optical and electrical properties of ZnO nanomaterials making them attractive for applications in a diverse range of disciplines including UV detectors, photocatalysis, sensors and antimicrobial coatings.

Morphological studies: The SEM micrographs presented in Fig. 2, captured at magnifications of 2 µm and 200 nm, revealed that the samples exhibit a granular and aggregated morphology. This has been indicated by several references that at the higher magnification (200 nm scale) the particles have polyhedral or near spherical shapes and therefore the quality of nucleation and to some extent growth was controlled, possibly as a result of the TAA dopant. The surfaces of the material exhibit roughness and densely packed surfaces suggesting good crystallinity and possibly porous zones, *i.e.* these are desired in applications such as catalysis, or sensors. In turn the difference on the various samples suggests varying dopant concentration, or synthesis conditions.

The grain size can estimate the size of several grains marked in the top-right image as sizes ranging from ~60 nm to ~120 nm, which suggests nanocrystalline. Doping with thioacetamide (TAA) significantly improved grain size uniformmity, suggesting its influence on nucleation and growth dynamics during reduction synthesis with Pluronic F127. The

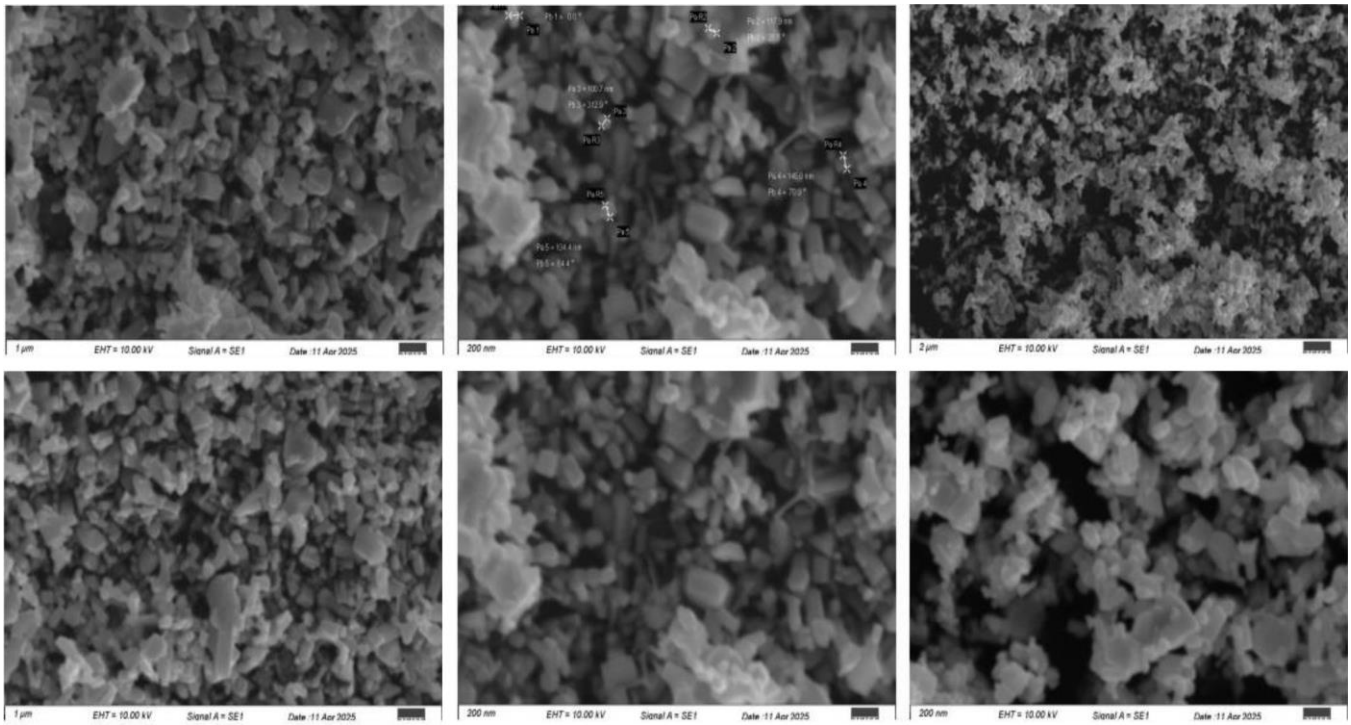

Fig. 2. SEM images of thioacetamide-doped zinc nitrate hexahydrate nanostructures

samples show a transition from polyhedral to spherical grains, indicating the isotropic growth, with high surface roughness enhancing surface area, which is ideal for catalytic and sensor applications. Moderate agglomeration is typical of doped systems due to thermochemical surface energy changes. Sample homogeneity varies, influenced by thermal treatments and doping levels. Thioacetamide (TAA) doping acts as a sulfur source, potentially forming ZnS phases or sulfur vacancies, while also controlling grain boundaries, reducing crystallite size, and enhancing surface uniformity. These modifications contribute to improved optical, catalytic and electrical properties by introducing defect states or altering the electronic band structure.

XPS analysis: X-ray photoelectron spectroscopy (XPS) confirmed the successful incorporation of thioacetamide (TAA) into $Zn(NO_3)_2 \cdot 6H_2O$, revealing the presence of zinc (Zn 2p at ~1022 eV and 1045 eV), oxygen (O 1s at ~531 eV), nitrogen (N 1s at ~400 eV), carbon (C 1s at ~285 eV), and sulfur (S 2p at ~164 eV). The binding energies, especially the Zn $2p_{3/2}$ at ~1021.5 eV and Zn $2p_{1/2}$ at ~1044.5 eV with ~23 eV spin–orbit splitting, confirm Zn^{2+} oxidation with no evidence of metallic Zn, suggesting that Zn remains in a nitrate-like environment possibly coordinated with TAA. The C 1s signal at ~285 eV corresponds to unexpected C–C/C–H moieties, while peaks at ~287–288 eV correspond to C=O or C–N functionalities from the amide group in TAA, confirming organic ligand integration (Fig. 3).

UV analysis: The UV–visible spectroscopic analysis revealed strong absorption in the UV region ($\lambda_{max} \approx 246$–260 nm), consistent with $\pi \rightarrow \pi^*$, $n \rightarrow \pi^*$ and ligand-to-metal charge-transfer (LMCT) transitions from sulfur or nitrogen lone pairs in TAA to Zn^{2+} orbitals. The exceptionally high absorbance (~4.0) and sharp post-peak decay suggest defect-mediated band-gap transitions and successful modification of electronic structure *via* hydrothermal synthesis (Fig. 4).

FT-IR studies: Further spectroscopic support comes from the FT-IR analysis, which detected O–H stretching bands at 3445–3440 cm^{-1}, indicating retained hydration. Vibrational signatures at 1117–1115 cm^{-1} (C–N) and 625–619 cm^{-1} (C=S) confirm coordination of TAA to Zn^{2+}, while modes observed around 490–480 cm^{-1} correspond to Zn–S or Zn–O bonds (Fig. 5). Together, these features validate the incorporation of TAA into the metal matrix.

Cyclic voltammetry (CV) studies: Electrochemical studies *via* cyclic voltammetry (I–V curves) show a nonlinear current–voltage response in the range –0.2 to 1.8 V. A sharp increase in current above ~1.2 V suggests carrier injection with low activation energy and likely Schottky or ohmic contact behaviour, while low-voltage flattening and small current fluctuations indicate trap-mediated conduction and defect related charge dynamics (Fig. 6). This behaviour highlights the role of TAA-induced defect states in facilitating enhanced charge transport, positioning the doped material as a promising candidate for sensors and optoelectronic devices.

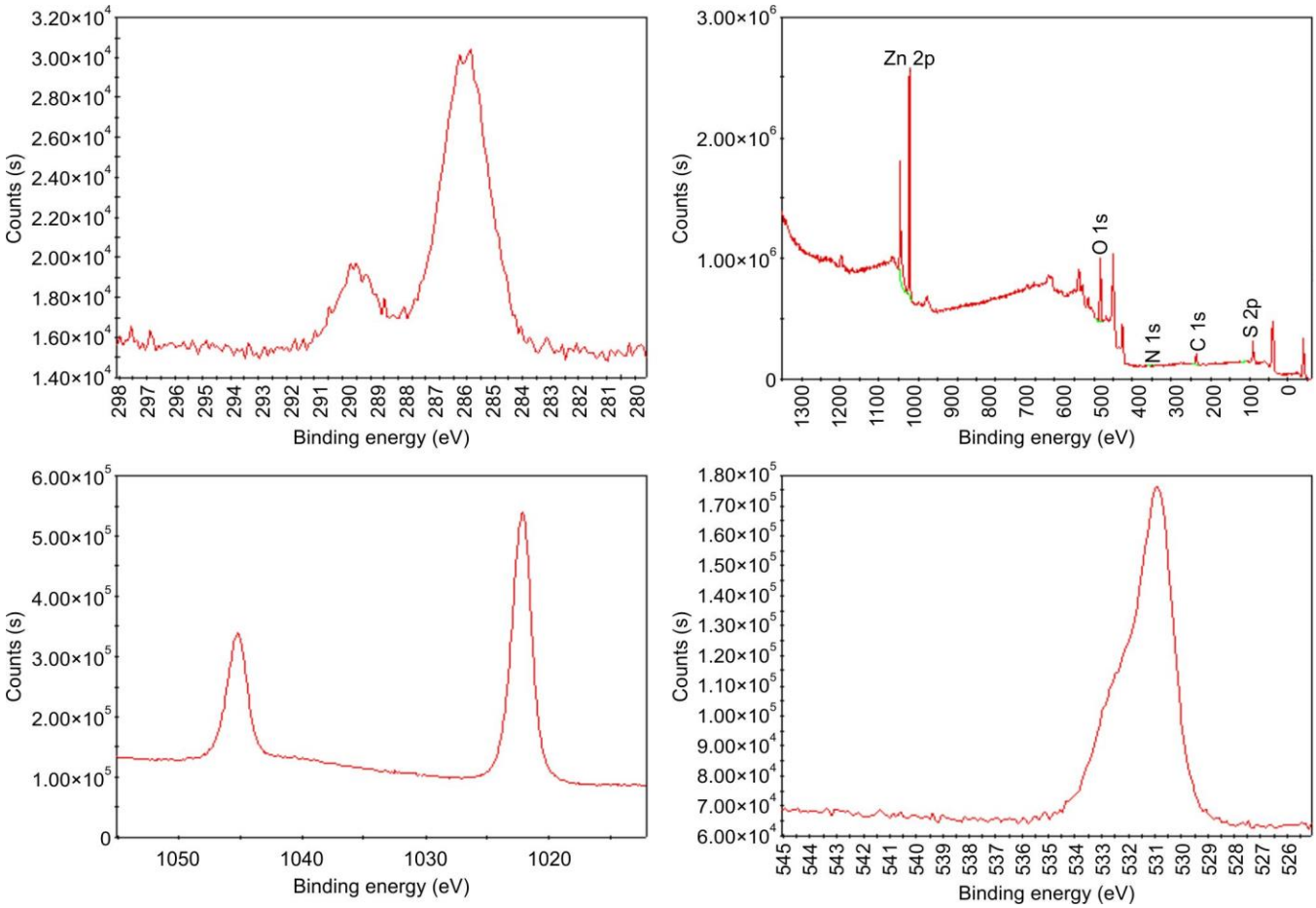

Fig. 3. XPS of thioacetamide-doped zinc nitrate hexahydrate nanostructures

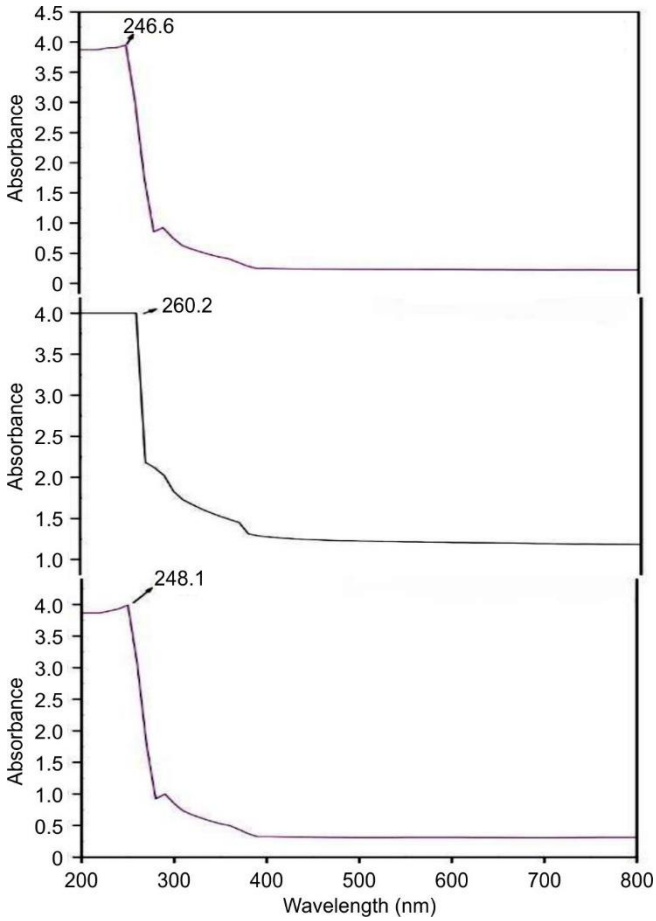

Fig. 4. UV-vis analysis of thioacetamide-doped zinc nitrate hexahydrate nanostructures

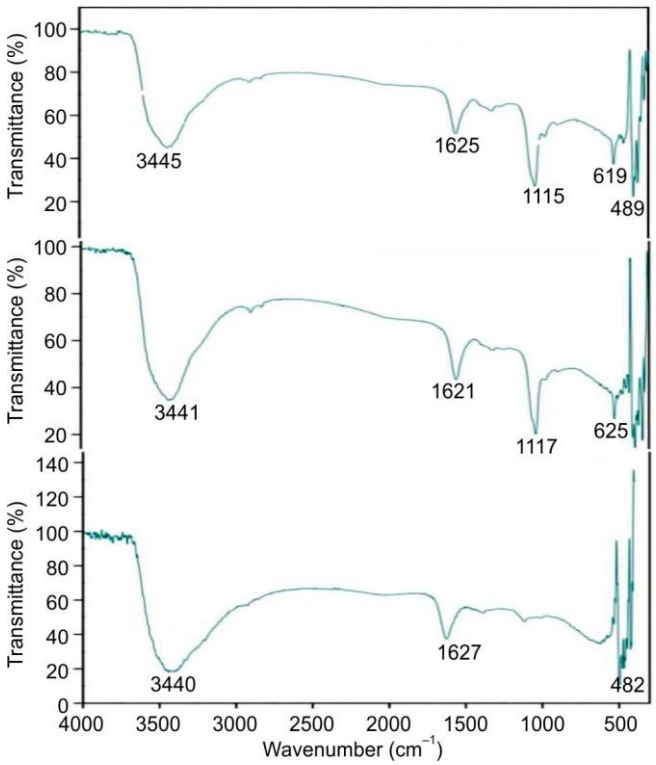

Fig. 5. FT-IR spectra of thioacetamide-doped zinc nitrate hexahydrate nanostructures

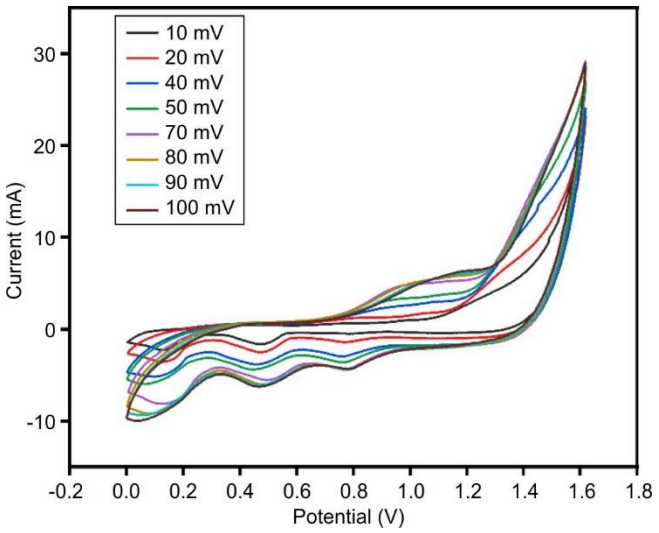

Fig. 6. CV graph of thioacetamide-doped zinc nitrate hexahydrate nanostructures

Galvanostatic charge-discharge (GCD): The GCD measurements in a 2-electrode setup yielded nearly symmetrical triangular curves (Fig. 7), indicative of dominant electric double-layer capacitive (EDLC) behaviour, alongside deviations pointing to Faradaic (pseudocapacitive) contributions. The minimal internal resistance (IR drop) and high coulombic efficiency reflect excellent conductivity and reversibility, suggesting suitability for energy storage applications. Thioacetamide doping appears to improve electron and ion transport kinetics and introduce redox-active defect sites, contributing to increased specific capacitance.

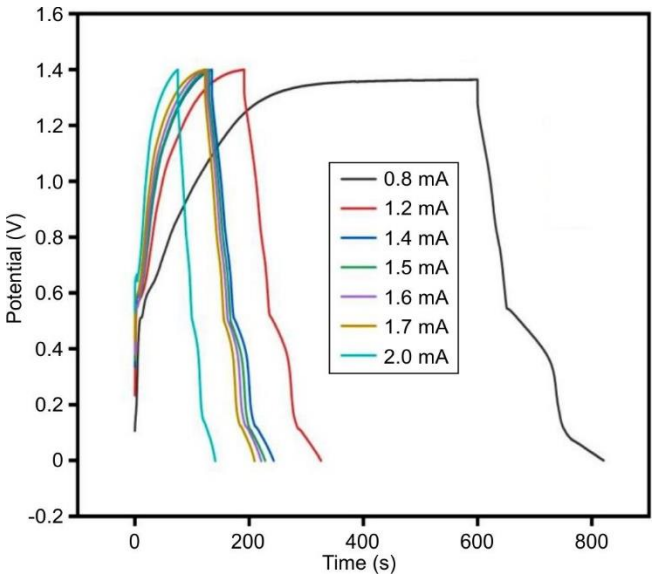

Fig. 7. GCD graph of thioacetamide-doped zinc nitrate hexahydrate nanostructures

The specific capacitance was calculated from the discharge portion of the GCD curves, with following equation:

$$C = \frac{I.\Delta t}{m.\Delta V.}$$

where I is the discharge current (A); Δt is the discharge time (s); ΔV is the potential window during which discharge occurs

(V) (IR drop removed); m is the active mass electrode material (g).

Conclusion

A thioacetamide-doped $Zn(NO_3)_2 \cdot 6H_2O$ was successfully synthesized *via* a simple hydrothermal method. The X-ray diffraction confirmed the crystalline phase of $Zn(NO_3)_2 \cdot 6H_2O$ with minor peak shifts indicating the successful incorporation of sulfur into the lattice. Scanning electron microscopy (SEM) revealed well-defined nanostructures with a porous morphology, favourable for electrochemical applications. X-ray photoelectron spectroscopy (XPS) confirmed the presence of Zn, O, N and S, verifying the chemical states and effective doping. UV–Vis spectroscopy showed a reduced band gap in the doped sample compared to the undoped one, suggesting enhanced electronic conductivity, while FTIR analysis identified characteristic functional groups and metal–dopant bonding environments. Electrochemical studies demonstrated excellent charge storage behaviour, with cyclic voltammetry (CV) curves exhibiting quasi-rectangular shapes characteristic of good capacitive performance. Galvanostatic charge–discharge (GCD) tests further revealed high specific capacitance, good rate capability, stable cycling and minimal IR drop, confirming the material's potential as a supercapacitor. Overall, the doped $Zn(NO_3)_2 \cdot 6H_2O$ exhibited promising structural, optical and electrochemical properties, supporting its applicability in next-generation energy storage systems.

CONFLICT OF INTEREST

The authors declare that there is no conflict of interests regarding the publication of this article.

REFERENCES

1. H.D. Weldekirstos, P. Girma, A. Tedla, N. Aberra and A. Negash, *Water Air Soil Pollut.*, **236**, 580 (2025); https://doi.org/10.1007/s11270-025-08217-2
2. S. Goel, N. Sinha, H. Yadav, A.J. Joseph, and B. Kumar, *Physica E*, **91**, 72 (2017); https://doi.org/10.1016/j.physe.2017.04.010
3. P.M. Patil, B. Sannakki, S.N. Mathad, E. Veena and S. Gandad, *Acta Period. Technol.*, **54**, 277 (2023); https://doi.org/10.2298/APT2354277
4. P.S. Krithika and J. Balavijayalakshmi, *Mater. Res. Express*, **6**, 105023 (2019); https://doi.org/10.1088/2053-1591/ab3828
5. H. Hajovsky, G. Hu, Y. Koen, D. Sarma, W. Cui, D.S. Moore, J.L. Staudinger and R.P. Hanzlik, *Chem. Res. Toxicol.*, **25**, 1955 (2012); https://doi.org/10.1021/tx3002719
6. M.C. Wallace, K. Hamesch, M. Lunova, Y. Kim, R. Weiskirchen, P. Strnad and S.L. Friedman, *Lab. Anim.*, **49(suppl)**, 21 (2015); https://doi.org/10.1177/0023677215573040
7. N.J. Waters, C.J. Waterfield, R.D. Farrant, E. Holmes and J.K. Nicholson, *Chem. Res. Toxicol.*, **18**, 639 (2005); https://doi.org/10.1021/tx049869b
8. J. Chilakapati, K. Shankar, M.C. Korrapati, R.A. Hill and H.M. Mehendale, *Drug Metab. Dispos.*, **33**, 1877 (2005); https://doi.org/10.1124/dmd.105.005520
9. Y.M. Koen, D. Sarma, H. Hajovsky, N.A. Galeva, T.D. Williams, J.L. Staudinger and R.P. Hanzlik, *Chem. Res. Toxicol.*, **26**, 564 (2013); https://doi.org/10.1021/tx400001x
10. Y. Zhang, Y. Jia, M. Li and L.A. Hou, *Sci. Rep.*, **8**, 9597 (2018); https://doi.org/10.1038/s41598-018-28015-7
11. S. Ahmed, D. Ibbotson, C. Somodi and P.J. Shamberger, *ACS Appl. Energy Mater.*, **2**, 530 (2024); https://doi.org/10.1021/acsaenm.3c00444
12. P. Li, Z.P. Xu, M.A. Hampton, D.T. Vu, L. Huang, V. Rudolph and A.V. Nguyen, *J. Phys. Chem. C*, **116**, 10325 (2012); https://doi.org/10.1021/jp300045u
13. M. Kasaeian, E. Ghasemi, B. Ramezanzadeh, M. Mahdavian and G. Bahlakeh, *Appl. Surf. Sci.*, **462**, 963 (2018); https://doi.org/10.1016/j.apsusc.2018.08.054
14. L. Wan, X. Wang, S. Yan, H. Yu, Z. Li and Z. Zou, *CrystEngComm*, **14**, 154 (2012); https://doi.org/10.1039/C1CE05805C
15. K. Oravcová and V. Danielik, *Acta Chim. Slov.*, **11**, 51 (2018); https://doi.org/10.2478/acs-2018-0008
16. C. Pholnak, C. Sirisathitkul and D.J. Harding, *J. Phys. Chem. Solids*, **72**, 817 (2011); https://doi.org/10.1016/j.jpcs.2011.04.005
17. P. Luo, F. Zhuge, Q. Zhang, Y. Chen, L. Lv, Y. Huang, H. Li, and T. Zhai, *Nanoscale Horizons*, **4**, 26 (2019); https://doi.org/10.1039/C8NH00150
18. B. R. Wahab, Y.S. Kim, K. Lee and H.S. Shin, *J. Mater. Sci.*, **45**, 2967 (2010); https://doi.org/10.1007/s10853-010-4294-x
19. D.D.S. Biron, V.D. Santos and C.P. Bergmann, *Mater. Res.*, **23**, e20200080 (2020); https://doi.org/10.1590/1980-5373-mr-2020-0080.
20. M.C. Akgun, Y.E. Kalay and H.E. Unalan, *J. Mater. Res.*, **27**, 1445 (2012); https://doi.org/10.1557/jmr.2012.92
21. A. Moezzi, M. Cortie and A.M. McDonagh, *Eur. J. Inorg. Chem.*, **2013**, 1326 (2013); https://doi.org/10.1002/ejic.201201244
22. L.A. Worku, M.G. Tadesse, R.K. Bachheti, A. Bachheti and A. Husen, *Int. J. Biol. Macromol.*, **267**, 131228 (2024); https://doi.org/10.1016/j.ijbiomac.2024.131228